Springer

KSME

Journal of Mechanical Science and Technology 32 (3) (2018) 1071~1078
www.springerlink.com/content/1738-494x(Print)/1976-3824(Online)
DOI 10.1007/s12206-018-0209-6

Numerical and experimental investigation of cavitation flows in a multistage centrifugal pump †

Md Rakibuzzaman[1], Kyungwuk Kim[1] and Sang-Ho Suh[2,*]

[1]*Graduate School, Department of Mechanical Engineering, Soongsil University, Seoul 06978, Korea*
[2]*Department of Mechanical Engineering, Soongsil University, Seoul 06978, Korea*

(Manuscript Received September 13, 2017; Revised October 24, 2017; Accepted October 24, 2017)

Abstract

Cavitation behavior is very important in pumps for long time operation. However, there is difficulty in predicting the cavitation phenomena of pumps by Computational fluid dynamics (CFD). In order to accurately ascertain cavitation behavior, a comparison between CFD and experimental data is a significant and essential process. The purpose of this study is to analyze cavitating behavior in multistage centrifugal pumps numerically and experimentally. For this investigation an experimental set up was used to obtain cavitation performance results. The CFD method was used to investigate the multistage centrifugal pump performance under developed cavitating conditions. The Reynolds-averaged Navier-Stokes (RANS) equations were discretized by the finite volume method. The two-equation SST turbulence model was adopted to account for turbulent flows. Numerical data were validated with experimental data and a good comparison of results was achieved. Numerically, cavitation performances were obtained for different pump stages and the effects on cavitation were described according to different NPSH (Net positive suction head). The occurrence of cavitation was also described according to $NPSH_{3\%}$ in the head drop lines and water vapor volume fraction on the impeller blade. The rapid drop in head at low NPSH was captured for different flow conditions. It was found that for stage to stage performance, the head drop changes could be related to losses inside the pump. It was also shown that the simulation results can truly represent the development of the attached sheet cavitation in the impeller.

Keywords: Multistage centrifugal pump; Cavitation performance; Cavitation model; RANS equation; Experiment; $NPSH_{3\%}$

1. Introduction

Cavitation is well recognized as a common physical phenomenon that may cause turbo-machines (Pumps, turbines etc.) malfunctioning due to improper design, and inlet conditions. It is the process of the formation of vapor bubbles which can be generated in relatively low pressure regions within a flow in centrifugal pumps [1]. Cavitation is a major cause of significant reduction in performance, as noticed by reduced mass flow rates, noise, vibrations, and erosion in centrifugal pumps [2]. It has been found that cavitation erosion is mainly related to the length of the attached sheet cavity, with the temperature of the liquid being pumped clearly affected by vapor pressure, as well as circumferential speed and the properties of the impeller material [3]. Therefore, in order to reduce these unavoidable effects, technology for accurately predicting and understanding cavitation is important in the development of centrifugal pumps [4].

Due to the importance of the cavitation phenomenon, numerical simulations have been widely used to investigate the cavitation flow field in turbomachinery such as pumps [5, 6]. In order to clarify and understand the behavior of cavity flow, cavity flow models and analytical methods for numerical simulations have been proposed [7, 8]. The mechanisms for cavitation have been extensively investigated and successful efforts have been made to establish cavitation and turbulence models for the simulation of cavitating flow [3, 9, 10].

There is an extensive amount of literature on experimental studies of cavitation and most of this research deals with hydrofoils. Arakeri and Acosta (1973) studied the viscous effects in the inception of cavitation and development on two axisymmetric bodies using the flow visualization method [11]. They found that incipient cavitation occurs within the region of separated flow and that the point of laminar separation and the leading edge of the cavity are closely related. Bakir et al. (2004) coupled the Rayleigh-Plesset equation to the flow solver and computed void fraction in the pump inducer [12]. Medvitz et al. (2002) performed a cavitation analysis in centrifugal pumps using multiphase CFD and pointed out the head inception and breakdown point [13]. Bruno et al. (2009) studied different NPSH characteristics in centrifugal pumps [1]. Kim et al. (2012) studied unsteady cavitation analysis in

*Corresponding author. Tel.: +82 2 820 0658, Fax.: +82 2 821 6758
E-mail address: suhsh@ssu.ac.kr
† This paper was presented at the ICCHM²T2017, Sejong Hotel, Seoul, Korea, May 28 – June 1, 2017. Recommended by Guest Editor Heuy Dong Kim.

centrifugal pumps and achieved a good comparison with experimental data [14]. Guo et al. (2015) recently has been investigated on the cavitation characteristics of a high-speed centrifugal pump with a splitter-blade inducer in both numerically by CFD and experimentally by visualization technique [15]. However, it is difficult to accurately predict cavitation in geometrically complex centrifugal pumps. Because of these difficulties many geometries are often simplified. A large number of hydrodynamics models are reported in 2D and 3D by using the CFD code and studied impeller diffuser interaction on the pump performance [16-18]. However, such models did not show a clear cavitating phenomenon in different pump stages. To account for the cavitation dynamics in a flexible manner, a transport equation model has recently been developed. In this approach the volume or mass fraction of a liquid and vapor phase is convicted. Singhal et al. (2002), Kunz et al. (2000), Shyy et al. (2002) have employed similar models based on this concept with differences in the source terms [19-21].

The present study is focused on investigating cavitation performances in multistage centrifugal pumps numerically and experimentally. An experimental set was made to get the pump performances at different flow operating conditions. Numerical simulations were used to validate multistage centrifugal pump model DR 20-60. In the numerical simulation for cavitation prediction, the Rayleigh-Plesset cavitation model, and a homogeneous liquid-vapor method were used. Governing equations were discretized by finite volume methods. The NPSH curves were estimated from the head drop lines for pump stages for different flows. The development of cavitation was also described according to $NPSH_{3\%}$ in the head drop lines and water vapor volume fraction in the pump.

2. Methods

2.1 Experimental method

An experimental test facility was conducted to analyze the pump performance of constant and variable speed drive operations. The test layout and experiment measurement system is shown in Fig. 1. The test facility was designed to meet ISO 5198 as shown in Fig. 1(b) [22]. The installed pump was a vertical multistage centrifugal (6-stages) type 11 kW, the water tank length was 2.5 m long, 4.5 m wide, 2.5 m high. Pipe diameter from the water tank was 100 mm, pipe diameter to the centrifugal pump was 50 mm, and pressure gauges were setup before and after 5D distance. The equipment used in the tests is shown in Table 1. The inlet side pressure gauge measurement range is -1~1 bar and the outlet side pressure gauge measurement range is 0~15 bar. A temperature sensor was installed at the pump inlet side. The pump head was measured by the difference between inlet and outlet pressures. Pump shaft torque was measured by torque meter which was connected to the signal amplifier.

An electromagnetic flow meter was set up to control and calculate the flow rate. Gate valves were installed at the inlet side and after the electromagnetic flow meter at the outlet of the pump. The gate valve after the electromagnetic flow meter was used to control the flow rate at a given constant speed during pump operation. The working fluid temperature was noted during cavitation testing.

Table 1. Pump experimental setup devices.

Equipment	Specification
Pump	DR 20-60
Motor	Vector motor 11 kW
Electromagnetic flow meter	BELIMO BLC100-EPIV
Pressure tank	PWB-DCP-100 LV-4 bar
Vacuum pump	30 Torr, 1050 L/min, 2.2 kW
Temperature sensor	EOMEGA

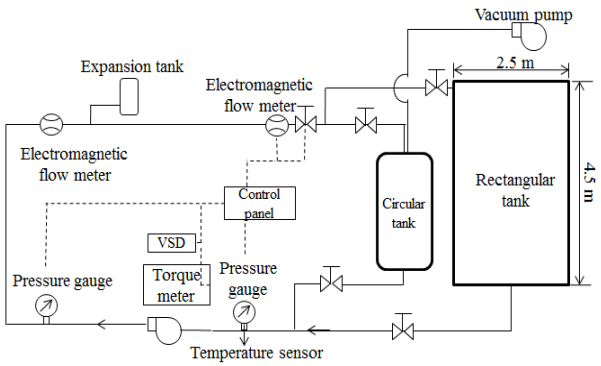

(a) Test layout

(b) Experimental facility of centrifugal pump system

Fig. 1. Centrifugal pump experiment layout and facilities.

During cavitation testing a valve throttling method was used to measure the NPSH for the pump being tested. NPSH testing was carried out by adjusting the pump capacity to the specified point. The suction valve was throttled to create vacuum at the pump suction, while the discharge valve was adjusted to maintain constant capacity. The test was repeated by further suction valve throttling until the head could not be maintained at constant capacity. The measurements were continued until the head was below the 3 % curve. $NPSH_r$ at 3 % head drop was measured and calculated. Finally, the test was

repeated for different capacities so that a complete $NPSH_{3\%}$ curve for the pump being tested could be drawn.

2.2 Numerical method

The fluid with cavitation is considered as a homogeneous, mixed medium of vapor and liquid. The governing equations are given as Eqs. (1) and (2);

$$\frac{\partial \rho_m}{\partial t} + \frac{\partial (\rho_m u_j)}{\partial x_j} = 0 \tag{1}$$

$$\rho_m \left(\frac{\partial u_i}{\partial t} + u_j \frac{\partial u_i}{\partial x_j} \right) = -\frac{\partial p}{\partial x_i} + \frac{\partial}{\partial x_j} \left[(\mu_m + \mu_t) \left(\frac{\partial u_i}{\partial x_j} + \frac{\partial u_j}{\partial x_i} \right) \right] \tag{2}$$

where ρ_m and μ_m are the mixture density and dynamic viscosity, calculated by the weighted average of each phase volume fraction, u is the velocity, p is the pressure, and μ_t is the turbulent viscosity respectively, subscripts i, j denote the coordinate directions, respectively. Mixture density and turbulence viscosity are defined by Eq. (3):

$$\rho_m = \rho_l \alpha_l + \rho_v (1 - \alpha_l)$$
$$\mu_m = \mu_l \alpha_l + \mu_v (1 - \alpha_l) . \tag{3}$$

The sum of all volume fractions must equal one.

$$\alpha_l + \alpha_g + \alpha_v = 1 . \tag{4}$$

The volume fractions were related to the mass fractions, f, for each component through the following relations as Eq. (5):

$$f_g = \frac{\alpha_g \rho_g}{\rho_m}, f_v = \frac{\alpha_v \rho_v}{\rho_m}, f_l = \frac{\alpha_l \rho_l}{\rho_m} = 1 - f_v - f_g \tag{5}$$

where f_v, f_g, f_l are the component mass fraction of the vapor, gas, and liquid; ρ_v, ρ_g, ρ_l are the component densities, α_v, α_g, α_l are the component of volume fractions. The liquid-vapor transfer due to the cavitation was modeled by a vapor volume fraction transport equation expressed as Eq. (6):

$$\frac{\partial}{\partial t}(\rho_m \alpha_m) + \frac{\partial}{\partial t}(\rho_m \alpha_m u_j) = \dot{S}_l \tag{6}$$

where $\alpha_v = 1 - \alpha_m$ and $\dot{S}_l = -\dot{S}_v$.

The source terms have units of (kg/s) where the source terms $\dot{S}_v$ and $\dot{S}_l$ account for mass exchange (Evaporation and condensation) between the vapor and liquid in the primary phases during cavitation. The formation and collapse of a cavity was modeled as a phase transformation. A cavitation model has been used based on the Rayleigh-Plesset equation (R-P) to estimate the rate of vapor production [12, 23]. Neglecting the second order term and surface tension force, the R-P equation is simplified to Eq. (7):

$$\frac{dR_B}{dt} = \sqrt{\frac{2}{3} \frac{|p_v - p|}{\rho_l}} . \tag{7}$$

This equation provided a physical method to incorporate the influence of the bubble dynamics into the cavitation model. The evaporation and conduction rate can be expressed as Eq. (8):

$$\dot{S}_v = F_{vap} \frac{3\alpha_{nuc}(1 - \alpha_v)}{R_B} \rho_v \sqrt{\frac{2}{3} \frac{|p_v - p|}{\rho_l}} \operatorname{sgn}(p_v - p)$$
$$\dot{S}_l = -F_{cond} \frac{3\alpha_v}{R_B} \rho_v \sqrt{\frac{2}{3} \frac{|p_v - p|}{\rho_l}} \operatorname{sgn}(p_v - p) \tag{8}$$

where α_{nuc} is the nucleation site volume fraction at 5.0×10^{-4}, R_B is the radius of a nucleation site at 1.0×10^{-6} m. The recommended values of the empirical parameters F_{vap} and F_{cond} are 50 and 0.01 for evaporation and condensation, respectively; if $p < p_v$ evaporation occurs and if $p > p_v$ condensation occurs.

2.3 Meshing and boundary conditions

The centrifugal model pump was used both with and without cavitation conditions for different stages as shown in Fig. 2. Fig. 3 shows meshing and domain of the pump. The model pump was meshed by ANSYS ICEM-CFX (Ansys Inc. 2013, USA) based on Finite volume methods (FVM) [24]. In order to reduce the influence of the grid number on the computational results, a grid dependency study (Impeller and diffuser) at the design point (24 m^3/hr) under non-cavitation condition was carried out for a steady state and it was found that the head deviation was less than 1 %. For non cavitating conditions the total meshing grids were 5265401 and 27529524. But for cavitating conditions, different pump stages were considered so the meshing grids and elements were different for each stage. Under the cavitation condition, the impeller domain was rotating on a y-axis at 3600 rpm with different flow operating conditions, and the diffuser was on a stationary domain. A frozen rotor was applied to couple the rotation and stationary domain. The inlet boundary's total pressure and mass flow rate was imposed at the outlet boundary. All boundary walls were assumed as smooth walls with non-slip conditions. The water temperature was set as 25 °C during the simulation, which indicates that the saturated vapor pressure is 3169 Pa. The *SST* turbulence model [24, 25] was used to solve the turbulence phenomena of the fluid. High resolution for the advection scheme, first order for the turbulence numeric and SIMPLEC algorithms were considered in the solver control. The steady state solution without cavitation was used as initial condition for steady state simulation with cavitation condition. The residual value was 1×10^{-5} controlled by convergence cri-

Table 2. Centrifugal pump design specifications.

Design flow rate	Rotation speed	Blade number	Impeller diameter	Outlet width
Q [m^3/hr]	N [rev/min]	Z	D_2 [m]	b_2 [m]
24	3600	6	0.1047	0.008

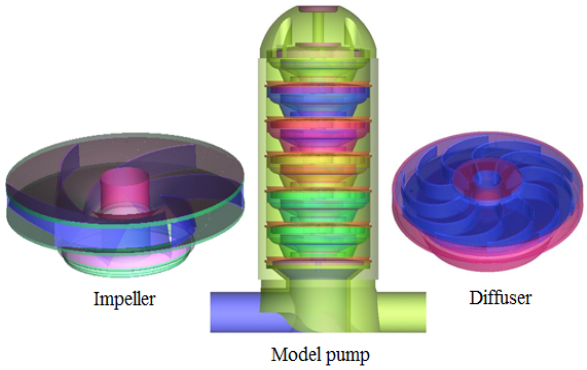

Fig. 2. Centrifugal model pump.

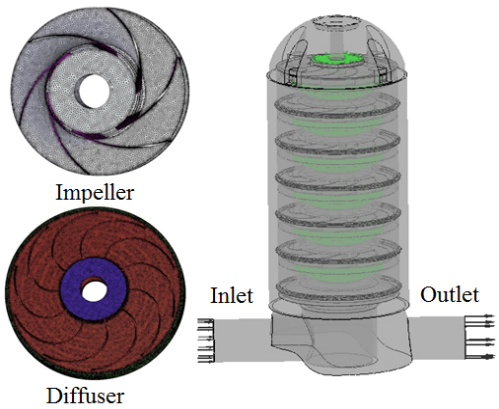

Fig. 3. Centrifugal pump meshing and domain for computation.

teria. Table 2 shows the design specification of the centrifugal pump model for the simulations.

3. Results and discussion

In what follows, four parameters were used to define the operating point and performance of the pump. These were head, power, efficiency, and NPSH; which are defined respectively here as:

$$H = \frac{p_2 - p_1}{\rho g} + \frac{V_2^2 - V_1^2}{2g} + (z_2 - z_1) \tag{9}$$

$$\eta = \frac{P_w}{P_s} = \frac{\rho Q g H}{\omega T} \tag{10}$$

$$\text{NPSH} = \frac{p_{in} - p_v}{\rho g}. \tag{11}$$

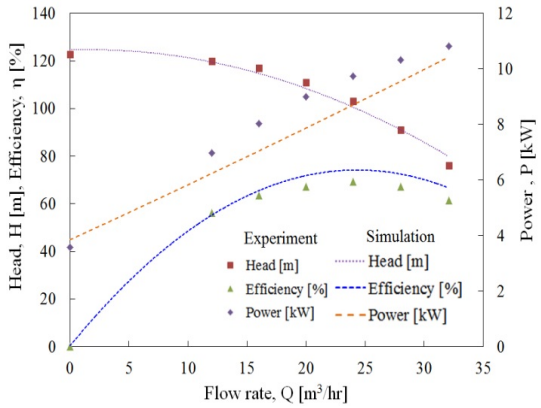

Fig. 4. Experiment and computational performances (Experimental uncertainty in N±3.65 rpm, Q±0.15 m^3/hr, H±0.109 and P±0.179 kW).

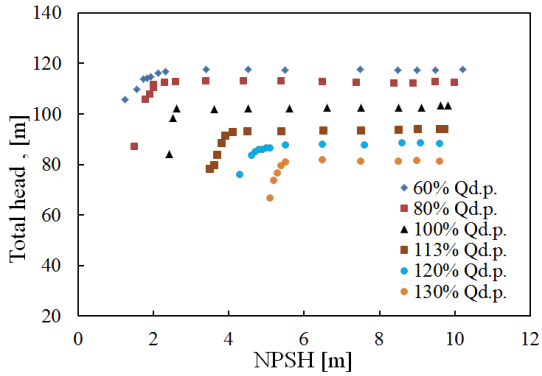

Fig. 5. Experimental results for different flow rates.

3.1 Validation of numerical results

In order to validate the numerical results, CFD results must be validated with experimental data. Fig. 4 shows the experimental and computational results with constant speed (3600 rpm) operation at design flow rate (24 m^3/hr). As shown, a good agreement between the two results was obtained at given flow rates. The maximum value of head was 9.7 % for the highest flow rate at 3600 rpm and the average value was 5.34 %. The maximum value of input power was 9.06 % and the average value was 6.35 %. The average efficiency was only 8.22 %. In Fig. 4 the deviation of the head seems to be smaller than that of the efficiency. The average head of the experimental and numerical simulations had only a 5.34 %, as was expected. In the simulation, leakage loss that occurred between the impeller and the diffuser/casing and the mechanical loss that occurs between the bearing and the shaft was not considered.

3.2 Cavitation performance

Fig. 5 shows the experimental values of the total head versus NPSH under six different flows operating conditions (60~130 % *Qd.p.*). In this figure *Qd.p.* is the flow rate at design point. The head drop lines were obtained by gradually

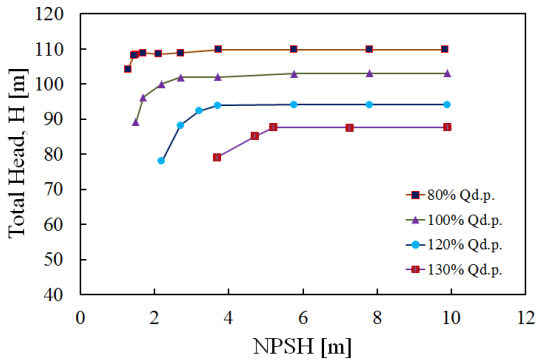

Fig. 6. Numerical results for different flow rates.

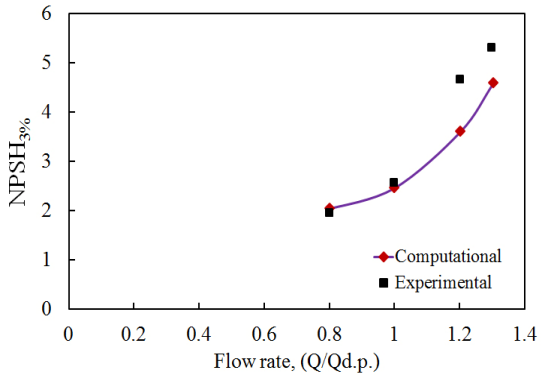

Fig. 7. Comparison of computational and experimental $NPSH_{3\%}$.

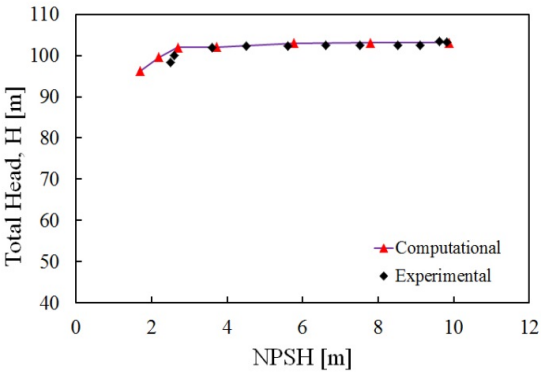

Fig. 8. Numerical results versus experimental results of head versus NPSH at design flow rate.

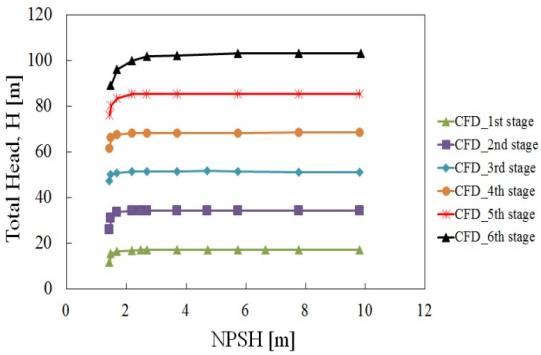

Fig. 9. Computed head versus NPSH for different pump stages at design flow rate.

reducing the suction pressure. The initial decrease of the NPSH had no effect on the head drop line because of pump and the total head remained unchanged. When the NPSH continued to decrease, the formation of vapor bubbles gradually increased resulting in a decrease of the total head which drops sharply at a lower NPSH. From these results, 3 % head drop accounted for cavitation conditions. Six flow rates were considered 60 %$Q_{d.p.}$, 80 %$Q_{d.p.}$, 100 %$Q_{d.p.}$, 113 %$Q_{d.p.}$, 120 %$Q_{d.p.}$ and 130 %$Q_{d.p.}$, for calculating NPSH, respectively.

At design flow rate, total head was constant but dropped steeply at the value of 2.57 m. When flow rate was reduced, cavitation occurred at lower NPSH. For flow rates of 60 %$Q_{d.p.}$ and 80 %$Q_{d.p.}$ the NPSH were 1.77 m and 1.94 m, respectively; but with increased flow rates, cavitation occurred at a rate greater than the design flow rate. At 113 %$Q_{d.p.}$, 120 %$Q_{d.p.}$ and 130 %$Q_{d.p.}$ flow rates the NPSH were 3.846 m, 4.64 m and 5.29 m, respectively. On the other hand, with the changed flow rate of 120 %$Q_{d.p.}$ the head was lower than the design flow rate but larger than the lower flow rate. In Fig. 5, it can be clearly seen that with changes in flow rate, the NPSH changes linearly until the 113 %$Q_{d.p.}$ flow rate. But after the 113 %$Q_{d.p.}$ flow rate, the cavitation number was not linear because of the occurrence of cavitation at higher NPSH. Fig. 6 shows the computed values of total head versus NPSH for six stages of pump. The predicted head drop shows a similar trend with experiment results. $NPSH_{3\%}$ is done by determining the cavitation point for a 3 % head drop at different operating points. Fig. 7 shows the $NPSH_{3\%}$ drop in flow rates of both experiment and computed results and illustrates that at design flow rate the 3 % head drop is showing almost similar values. $NPSH_{3\%}$ curve shows frequently towards the origin of the coordinates and increases steadily with increasing flow rates because cavitation occurs at higher NPSH beyond the design point and the occurrence of cavitation could be affected on the pump impeller pressure side. If the pump was operated under the required $NPSH_{3\%}$, the formation of cavitation pitting on the impeller blade may be possible.

It could be predicted from the above results that-, liquid-vapor phase flow prevails in a large portion of the impeller blades. Fig. 8 shows a comparison of experimental and computed total head versus NPSH. Both results show good agreement.

On the other hand, it is reported that-, for the same impeller diameter for all stages, the $NPSH_{3\%}$ could be related to the drop in the head of the first stage [26]. Therefore, the cavitation performances for different pump stages have been investigated. Fig. 9 shows the computed results for different pump stages (1st to 6th stages) at design flow rate at a given rotational speed of 3600 rpm. As can be seen in Fig. 9, the initial head drop line for all stages remain unchanged, but there is a slightly changed 3 % head drop for each pump stages. This

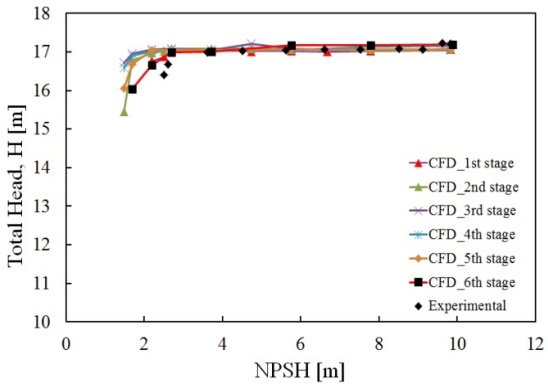

Fig. 10. Predicted and experimental head drops comparison with first stage pump.

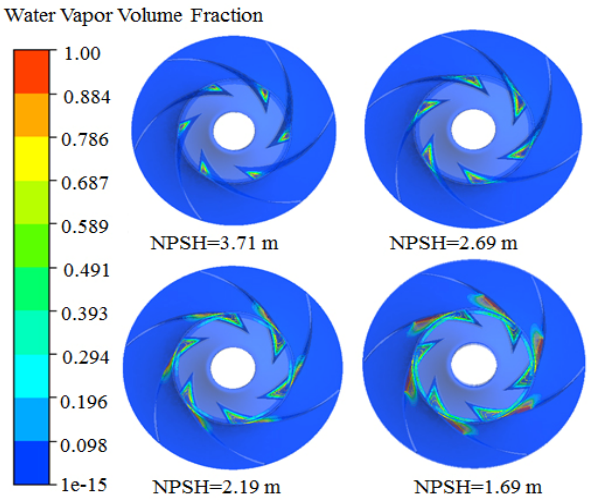

Fig. 11. Cavitation phenomena in the pump impeller (Q/Qd.p. = 1.0, sixth stages).

could be related with pump stage to stage head loss. For better understanding a comparison was made for each stage with experimental results considering single stage cavitation performance. Fig. 10 shows the numerical simulations and experimental head drops comparison with single stage pump. Fig. 10 clearly shows that the computed cavitation performances for single stage and sixth stages 3 % head drops were almost the same, but for the third and fourth stages head drops were slightly changed from the first and sixth stages. The fifth stages 3 % head drop performance was lower than the third and the fourth stages but higher than first and six stages. In the experiment, the head drops rocketry. For stage to stage performance, the head drop changes could be related to losses inside the pump. In a further, comparison with experiment, numerical simulation did not consider leakage loss that occurred between the impeller and the diffuser/casing and the mechanical loss that occurs between the bearing and the shaft.

3.3 Cavitation analysis

The cavity volume fraction with different NPSH at the design flow rate was clearly observed in the developed model pump impeller through numerical simulations (Figs. 6 and 11). Cavitation bubbles grew and appeared first at the suction zone near the blade's leading edge. The pressure in this section was smaller than in the hub due to the centrifugal force of the pump impeller. As such the cavitation became larger from shroud to hub and the cavitation rapidly grew from the suction side to the pressure side. When the NPSH value decreased, the cavitation length increased from leading suction edge to trailing edge, which was a significant factor on the impeller blades. For NPSH = 3.71 m, the pump head began to drop. In this case the pressure loading was increased on the impeller blade. For NPSH = 1.69 m the cavitation length was almost fully formed on the blade impeller and the length of bubble cavities increased from the leading edge to the trailing edge. With the decreasing net positive suction head, visual observation indicated that the attached cavitation extension gradually increased. At this stage, obstruction of; the flow channel by the cavities had almost began, which could form a pitting on the blade, and could block the internal flow of the model pump. In this case the influence of cavitation on the loading distribution of the pressure would be reduced both at the leading and trailing edge. Hence, head dropped by the results of this cavitation phenomenon and corrosion could have occurred on the impeller blade.

4. Conclusions

This study was based on cavitation performances in a multistage centrifugal pump with a constant speed drive system. A model DR 20-60 multistage centrifugal pump was installed with a designed layout to get the pump performances at a constant and variable speed drive system. The experimental results were investigated and validated with numerical simulations data for model validation, effectiveness and reliability of the pump. Also, in cavitating conditions, the 3 % head drop showed a good comparison between experiment and numerical values. For computation, a Rayleigh-Plesset cavitation model was used to simulate the ANSYS-CFX code. Steady simulations were performed with a shear stress transport turbulence model to perform the cavitation phenomena at different flow rates at a given rotational speed. The propagation of the cavitation on the impeller blade was observed. The cavitation head drop lines were estimated at different operating conditions. The performances were described according to different net positive suction head. The computed head drops of $NPSH_{3\%}$ were clearly estimated. Attached cavitation occurred on the pump impeller blade at the lower suction head. The results show that attached cavitation can directly lead to losses in efficiency, especially for flow rates inside the cavitation zone. Cavitation first occurred at the suction leading edge on the impeller blades. When the value of NPSH decreased, the length of cavities grew to a significant extent. The decreased

head drop obstructed flow channel by the cavities, which could form pitting on the impeller. Further, the cavitation performances for different pump stages were investigated and compared with the experimental results. The results indicated in numerical simulation did not consider head leakage loss that occurred in the impeller and the diffuser/casing and the mechanical loss.

Acknowledgment

This work (Grants No. 201615081279) was supported by Business for Cooperative R&D between industry, academy, and research institute funded Korea Small and Medium Business Administration for the Promotion of Science.

Nomenclature

g : Acceleration due to gravity [m/s^2]
$NPSH$: Net positive suction head [m]
ω : Angular velocity [rad/s]
T : Torque [N·m]
α : Volume fraction
μ : Viscosity [Pa·s]
P_{in} : Suction pressure [Pa]
P_v : Vapour pressure [Pa]

Subscripts

i,j : Tensor indices
l : Liquid
m : Mixture
g : Gas
$1,2$: Inlet, exit

References

[1] B. Schiavello and F. C. Visser, Pump cavitation—various NPSHR criteria, NPSHA margins, and impeller life expectancy, *Proc. of the 25th International Pump Users Symposium*, Turbomachinery Laboratory, Texas A&M University, College Station, TX (2009) 113-144.

[2] Japan Association of Agriculture Engineering Enterprises, *Pumping station engineering hand book*, Tokyo (1991) 50-90.

[3] C. E. Brennen, *Hydrodynamics of pump*, Oxford University Press, Oxford, UK (1994).

[4] B. R. Shin et al., Application of preconditioning method to gas-liquid two-phase flow computations, *ASME J. of Fluids Eng.*, 126 (2004) 605-612.

[5] B. Pouffary, R. F. Patella, J. L. Reboud and P. L. Lambert, Numerical simulation of 3D cavitating flows analysis of cavitation head drop in turbomachinery, *ASME J. of Fluids Eng.*, 130 (2008) 301-310.

[6] D. O. Coutier, P. R. Fortes and J. L. Reboud, Evaluation of the turbulence model influence on the numerical simulations of unsteady cavitation, *ASME J. of Fluids Eng.*, 125 (2003) 38-45.

[7] I. Senocak and W. Shyy, Numerical simulation of turbulent flows with sheet cavitation, *Int. Symposium on Cavitation*, A7 (2001) 2-8.

[8] M. P. Fard and E. Roohi, Transient simulations of cavitating flows using a modified Volume of fluid (VOF) technique, *Int. J. of Computational Fluid Dynamics*, 22 (2008) 97-114.

[9] D. O. Coutier, P. R. Fortes, J. Reboud, M. Hofmann and B. Stoffel, Experimental and numerical studies in a centrifugal pump with two-dimensional curved blades in cavitating condition, *ASME J. of Fluids Eng.*, 125 (2003) 970-978.

[10] B. R. Shin, A high resolution numerical scheme for a high speed gas-liquid two-phase flow, *Journal of Mechanical Science and Technology*, 25 (5) (2011) 1373-1379.

[11] V. H. Arakeri and A. J. Acosta, Viscous effects in the inception of cavitation on axisymmetric bodies, *ASME J. Fluids Eng.*, 95 (1973) 519-528.

[12] F. Bakir, R. Rey, A. G. Gerber, T. Belamri and B. Hutchinson, Numerical and experimental investigations of the cavitating behavior of an inducer, *Int. J. of Rotating Machinery*, 10 (2004) 15-25.

[13] R. B. Medvitz et al., Performance analysis of cavitating flow in centrifugal pumps using multiphase CFD, *ASME J. of Fluids Eng.*, 124 (2) (2002) 377-383.

[14] D. H. Kim, W. G. Park and C. M. Jung, Numerical simulation of cavitating flow past axisymmetric body, *Int. J. of Naval Architect Ocean Engineering*, 4 (3) (2012) 256-266.

[15] X. M. Guo, L. Zhu, Z. C. Zhu, B. L. Cui and Y. Li, Numerical and experimental investigations on the cavitation characteristics of a high-speed centrifugal pump with a splitter-blade inducer, *Journal of Mechanical Science and Technology*, 29 (1) (2015) 259-267.

[16] D. Croba and J. L. Kueny, Numerical calculation of 2D, Unsteady flow in centrifugal pumps: Impeller and volute interaction, *Int. J. for Numerical Methods in Fluids*, 22 (1996) 467- 481.

[17] Y. K. P. Shum, C. S. Tan and N. A. Cumpsty, Impeller-diffuser interaction is a centrifugal compressor, *Journal of Turbomachinery*, 122 (4) (2000) 777-786.

[18] A. Akhras, M. El Hajem, J.-Y. Champagne and R. Morel, The flow rate influence on the interaction of a radial pump impeller and the diffuser, *Int. J. of Rotating Machinery*, 10 (4) (2004) 309-317.

[19] A. K. Singhal, M. M. Atavale, H. Li and Y. Jiang, Mathematical basis and validation of the full cavitation model, *ASME J. of Fluids Engineering*, 124 (3) (2002) 617-624.

[20] R. F. Kunz et al., A preconditioned Navier-Stokes method for two phase flows with application to cavitation prediction, *Computers and Fluids*, 29 (8) (2000) 849-875.

[21] I. Senocak and W. Shyy, A pressure based method for turbulent cavitating flow components, *Journal of Computational Physics*, 179 (2) (2002) 363-383.

[22] *ISO 5198: 1987 (E)*, Centrifugal, mixed flow and axial pumps-code for hydraulic performance tests-precision class,

International Standard.
[23] C. E. Brennen, *Cavitation and bubble dynamics,* Oxford University Press, UK (1995).
[24] Ansys Inc., *ANSYS-CFX (CFX introduction, CFX reference guide, CFX tutorials, CFX-pre user's guide, CFX-solver manager user's guide, theory guide)*, release 14.5, USA (2013).
[25] N. J. Georgiadis, D. A. Yoder and W. B. Engblorn, Evaluation of modified two-equation turbulence models for jet flow predictions, *AIAA Journal*, 44 (12) (2006) 3107-3114.
[26] J. F. Gulich, *Centrifugal pump,* 3rd Edition, Springer, London (2014).

Md Rakibuzzaman is a Researcher at Soongsil University, Seoul, Korea. He is currently a Ph.D. student at Soongsil University under the supervision of Prof. Dr. -Ing. Sang-Ho Suh. His research interests include cavitation phenomena in turbo machinery and biomedical engineering.

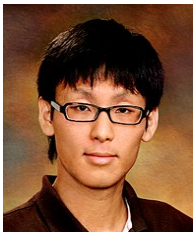

Kyungwuk Kim is a Researcher at Soongsil University, Seoul, Korea. He is currently a Ph.D. student at Soongsil University under the supervision of Prof. Dr. -Ing. Sang-Ho Suh. His research interests include development of turbo machinery.

Sang-Ho Suh is a Professor of Dept. of Mechanical Engineering at Soongsil University, Seoul, Korea. He received his Ph.D. degree from Stuttgart University in 1989. He has been teaching at Soongsil University since 1990. His research contributions were in the field of fluid machinery and Bio-fluid engineering. He is currently working on biomedical engineering research includes biofluid circulations (blood, urine and air flows in arteries, ureter, upper airway), development of biomedical devices, and industrial application researches of performance evaluation of pumps and hydraulic turbines, development of automatic waste collecting system, Pneumatic capsule pipeline (PCP).